Distinct Kinetic and Molecular Requirements Govern CD44 Binding to Hyaluronan versus Fibrin(ogen)

Phrabha S. Raman,[†] Christina S. Alves,[†] Denis Wirtz,[†‡§¶] and Konstantinos Konstantopoulos[†‡§¶*]
[†]Department of Chemical and Biomolecular Engineering, [‡]Johns Hopkins Institute for NanoBioTechnology, [§]Johns Hopkins Physical Sciences-Oncology Center, and [¶]Center of Cancer Nanotechnology Excellence, The Johns Hopkins University, Baltimore, Maryland

ABSTRACT CD44 is a multifunctional glycoprotein that binds to hyaluronan and fibrin(ogen). Alternative splicing is responsible for the generation of numerous different isoforms, the smallest of which is CD44s. Insertion of variant exons into the extracellular membrane proximal region generates the variant isoforms (CD44v). Here, we used force spectroscopy to delineate the biophysical and molecular requirements of CD44-HA and CD44-fibrin(ogen) interactions at the single-molecule level. CD44v-HA and CD44s-HA single bonds exhibit similar kinetic and micromechanical properties because the HA-binding motif on CD44 is common to all of the isoforms. Although this is the primary binding site, *O*- and *N*-linked glycans and sulfation also contribute to the tensile strength of the CD44-HA bond. The CD44s-fibrin pair has a lower unstressed dissociation rate and a higher tensile strength than CD44s-fibrinogen but is weaker than the CD44-HA bond. In contrast to CD44-HA binding, the molecular interaction between CD44 and fibrin(ogen) is predominantly mediated by the chondroitin sulfate and dermatan sulfate on CD44. Blocking sulfation on CD44s modestly decreases the tensile strength of CD44s-fibrin(ogen) binding, which is in stark contrast to CD44v-fibrin interaction. Collectively, the results obtained by force spectroscopy in conjunction with biochemical interventions enable us to delineate the biophysical parameters and molecular constituents of CD44 binding to hyaluronan and fibrin(ogen).

INTRODUCTION

CD44 is a multitasking protein that plays a pivotal role in a number of physiological processes, including inflammation, hematopoiesis, wound healing, and cancer metastasis. CD44 is a type I transmembrane glycoprotein encoded by a single gene, and comprises at least 20 exons (1). Exons 1–5, 16–18, and 20 are spliced together to form the smallest CD44 transcript, known as the standard CD44 isoform (CD44s; Fig. 1 *A*). At least 10 exons (exons 6–15, typically identified as v1–v10) can be alternatively spliced and inserted at a single site within the membrane-proximal portion of the extracellular domain to give rise to multiple variant isoforms of CD44 (Fig. 1 *A*). CD44 undergoes extensive post-translational modifications resulting from the attachment of carbohydrates to *N*- and *O*-linked glycosylation sites of the extracellular domain, and of glycosaminoglycans (GAGs) such as chondroitin sulfate (CS), dermatan sulfate (DS) (2), heparan sulfate (3), and keratan sulfate (4) (Fig. 1 *A*).

CD44 is the major cell surface receptor for hyaluronan (or hyaluronic acid (HA)), a nonsulfated glycosaminoglycan (GAG) that is composed of repeating units of D-glucuronic acid and *N*-acetyl-D-glucosamine (1). HA is a major component of the extracellular matrix in most mammalian tissues, and is upregulated on the surface of endothelial cells upon proinflammatory stimuli (5,6). CD44-HA binding has been implicated in the migration of activated leukocytes and lymphocytes to sites of inflammation, presumably by attachment to vascular endothelial cell walls (7,8). CD44-HA interactions also play a key role in matrix-dependent migration pertaining to inflammation and cancer metastasis. Although both the standard and variant isoforms bind HA, some studies have suggested that CD44s binds more efficiently than CD44v (9–11), whereas others have shown the opposite (12). These conflicting data may be attributed to subtle changes in the expression levels of CD44s versus CD44v on the cell surface. To eliminate the potential effects of differential expression of CD44s versus CD44v on the efficiency of HA binding, we sought to determine the kinetic and micromechanical properties of the aforementioned pairs at the single-molecule level. To that end, we used a micromanipulation method based on single-molecule force spectroscopy to investigate these biomolecular interactions at short and long dwell times, thereby simulating the receptor-ligand encounter time at high and low shear regimes, respectively (13–15). HA immobilized on a cantilever tip was brought into contact for prescribed durations of contact with immunopurified CD44 incorporated into lipid vesicles and layered onto a polyethyleneimine (PEI)-cushioned glass slide. CD44v-HA and CD44s-HA bonds display a similar tensile strength, unstressed dissociation rate, and reactive compliance, which is explained by the fact that the HA-binding motif is common to all CD44 isoforms. Moreover, *O*- and *N*-linked glycans and sulfation contribute to the tensile strength of CD44-HA binding.

CD44 also interacts with fibrin and fibrinogen (16–18). However, it remains to be determined how the different molecular constituents influence the biophysical properties of these receptor-ligand bonds at the single-molecule level. Using force spectroscopy, we determined that the

Submitted April 26, 2012, and accepted for publication June 18, 2012.

*Correspondence: kkonsta1@jhu.edu

Editor: Petra Schwille.

0006-3495/12/08/0415/9 $2.00

http://dx.doi.org/10.1016/j.bpj.2012.06.039

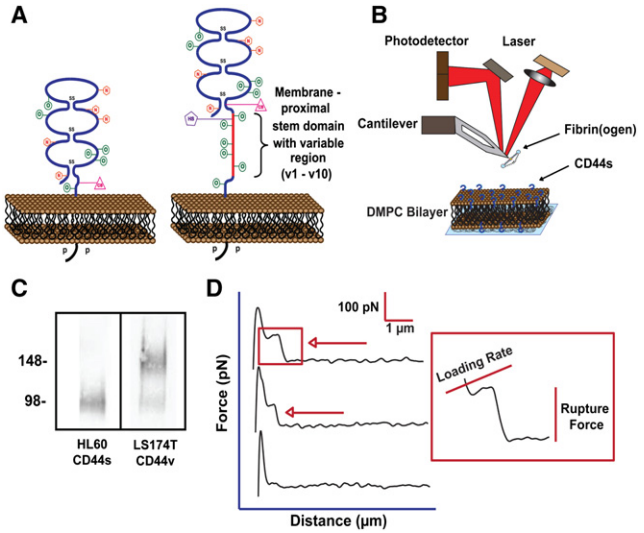

FIGURE 1 Single-molecule force spectroscopy as used to probe the biomechanical properties of CD44s-fibrin(ogen) bonds. (*A*) Schematic diagram of the standard and variant isoforms of CD44. Orange hexagons represent putative sites of *N*-linked glycosylation; green circles represent putative sites for *O*-linked glycosylation (SS, disulfide bond; P, serine phosphatases). (*B*) Schematic diagram of the MFP used to investigate the kinetic and micromechanical properties of receptor-ligand interactions at single-molecule resolution. (*C*) CD44s was immunoprecipitated from HL60 human myeloid leukemia cells, and CD44v was immunoprecipitated from LS174T colon carcinoma cells and subjected to SDS-PAGE under reducing conditions, followed by Western blotting using the anti-CD44 mAb 2C5. (*D*) Typical force-distance traces acquired from force spectroscopy experiments in which fibrin or fibrinogen immobilized on a cantilever tip was brought into contact hundreds of times with immunopurified CD44s incorporated into lipid vesicles and layered onto a PEI-cushioned glass slide. The red arrows in the first two curves indicate two distinct CD44s-fibrin rupture events. The rupture event in the red box is enlarged on the right to show the drop in the force. The slope before rupture multiplied by the retraction velocity gives the loading rate. The third curve is typically obtained when there is no binding. The scale bar for the three curves is also indicated.

CD44s-fibrin bond is mechanically stronger than the CD44s-fibrinogen pair, but more labile than CD44-HA. The CD44-fibrin(ogen) molecular recognition is predominantly dependent on CS and DS GAGs on CD44. Of note, sulfation exerts opposite effects on the biophysical properties of CD44s-fibrin versus CD44v-fibrin bonds. Taken together, our single-molecule characterization studies resolve the differences documented in the literature pertaining to CD44-HA interactions, and delineate the critical role of the molecular constituents involved in CD44 binding to its counter-receptors.

MATERIALS AND METHODS

Reagents and monoclonal antibodies

Fibrinogen (von Willebrand factor, plasminogen, and fibronectin free) was obtained from Enzyme Research Laboratories (South Bend, IN). Thrombin, chondroitinase ABC (*Proteus vulgaris*), benzyl 2-acetamido-2-deoxy-α-D-galactopyranoside (benzyl-GalNAc), HA, and sodium chlorate were obtained from Sigma Chemical Company (St. Louis, MO). Sialidase (*Vibrio cholerae*) was obtained from Roche Applied Science, and PNGaseF was obtained from New England Biolabs (Ipswich, MA). Anti-human CD44 monoclonal antibody (mAb) 2C5 was obtained from R&D Systems (Minneapolis, MN). The anti-human CD44 mAb 515 was obtained from BD Biosciences (San Jose, CA). PEI was obtained from Polysciences (Warrington, PA), and 1,2-Dimyristoyl-*sn*-glycero-3-phosphocholine (DMPC) was obtained from Avanti Polar Lipids (Alabaster, AL).

Cell culture, whole-cell lysis, and immunoprecipitation

LS174T human colon adenocarcinoma cells and HL60 human myeloid cells were obtained from the American Type Culture Collection (Manassas, VA) and cultured in the recommended medium. LS174T or HL60 whole-cell lysate was prepared by membrane disruption using 2% Nonidet P-40 (Sigma Chemical) followed by differential centrifugation. CD44v was immunoprecipitated from LS174T colon carcinoma cell lysate with the anti-CD44 mAb 2C5. Of note, LS174T metastatic colon carcinoma cells express predominantly the CD44 variants v3, v5, v7, and v8, whereas the variant regions v4, v6, and v10 are present in a small percentage of isoforms (19). CD44s was immunoprecipitated from HL60 human myeloid cell lysates with anti-CD44 mAb 515 using recombinant protein G-agarose beads (Invitrogen) (16,19,20).

Lipid bilayer preparation

To prepare lipid solutions, we dissolved 8 mg of DMPC in 8 ml of lipid buffer B (20 mM Tris-HCl, 50 mM NaCl, 1 mM $CaCl_2$, 0.1% (w/v) Triton X-100). To 400 μl of lipid solution, 100 μl of CD44s or CD44v at a concentration of 100 μg/ml was added and incubated at 37°C for 2 h (21). The lipid-protein solution was transferred to a 10 kDa MWCO dialysis cassette and dialyzed against 1L of lipid buffer A (20 mM Tris-HCl, 50 mM NaCl, 1 mM $CaCl_2$) three times for 12 h each. Lipid-protein solutions were then stored at 4°C under argon for up to 1 month. To prepare bilayers, glass slides were cleaned with plasma oxygen for 5 min and immediately submerged in a solution of 100 ppm PEI in 0.5 mM KNO_3 for 20 min before they were rinsed with deionized water and dried with nitrogen. The slides were further dried in a vacuum desiccator overnight before use. The PEI-coated slides were then incubated with a 4 μl droplet of the lipid-protein solution for 1–2 h under a slightly dampened towel to prevent complete dehydration. The slides were then rinsed with Hank's balanced salt solution (HBSS) and flooded with HBSS for use in molecular force probe (MFP) experiments. In select experiments, the DMPC-CD44s solution was premixed with 20 μg/ml Hermes-1 anti-CD44 mAb before incubation on the glass slide (15).

SDS-PAGE and Western blotting

Immunoprecipitated CD44v and CD44s were resolved on a 4–20% Tris-HCl Criterion gel (Bio-Rad) using Tris/glycine running buffer under reducing conditions. Resolved proteins were transferred to immunoblot polyvinylidene difluoride membranes and stained with the anti-CD44 mAb 2C5 (Fig. 1 *C*) (16,20).

Treatments with inhibitors and enzymes

To degrade all forms of CS and DS, we incubated CD44s-incorporated lipid bilayers for 1 h at 37°C with 1 U/ml *P. vulgaris* chondroitinase ABC before obtaining force spectroscopy measurements (15,16). To cleave *N*-linked glycans from CD44, immunopurified LS174T CD44v and HL60 CD44s were treated with PNGase F for 1 h at 37°C according to the manufacturer's

specification (16,19). Before conducting metabolic inhibitor studies, we pretreated the LS174T and HL60 cell suspensions (10^7 cells/ml) with 0.1 U/ml *V. cholerae* sialidase for 60 min at 37°C to remove terminal sialic acid residues and ensure de novo synthesis of newly generated HECA-452 reactive carbohydrate structures. Subsequently, LS174T or HL60 cells were cultured for 48 h at 37°C in medium containing 2 mM benzyl-GalNAc to inhibit *O*-linked glycosylation (16,19,20). To inhibit sulfation, CD44v was immunopurified from LS174T colon carcinoma cells, which were cultured for 48 h at 37°C in medium containing 60 mM sodium chlorate, and CD44s was immunopurified from HL60 human myeloid cells that were cultured in medium containing 20 mM sodium chlorate (16). DPBS was used as a diluent control.

Cantilever functionalization

To obtain a surface that would readily bind soluble proteins, we silanized MFP cantilevers (Bruker Nano, Camarillo, CA) with 2% 3-aminopropyl-triethoxysilane (13–15,22). The cantilevers were then incubated in a 5 μg/ml solution of fibrinogen in DPBS containing 50-fold molar excess of the cross-linker *bis*(sulfosuccinimidyl) suberate (BS^3; Pierce, Rockford, IL) for 30 min followed by quenching with Tris buffer. To form fibrin, the cantilever tips were incubated with 2 U/ml thrombin in DPBS for 2 h at 37°C, followed by immersion in Tris buffer to block nonspecific interactions (15). In control experiments, the silanized cantilevers were incubated with a 2 U/ml solution of thrombin in DPBS containing BS^3 for 30 min followed by quenching with Tris buffer. Carbodiimide chemistry using 1-ethyl-3-(3-dimethylaminopropyl) carbodiimide) and N-hydroxysulfosuccinimide (both from Pierce, Rockford, IL) was employed to activate the carboxylic groups on HA to form a covalent bond with the amine groups of the silanized tips according to the manufacturer's specifications (23).

Single-molecule force spectroscopy, data acquisition, and analysis

We conducted experiments using an MFP (Asylum Research, Santa Barbara, CA) (13–15,22). We calibrated the softest triangular cantilever (C type cantilever, MLCT probes) using the thermal noise amplitude and measured its deflection by laser reflection onto a split photodetector (Fig. 1 *B*). The distance between the cantilever and the DMPC-CD44 bilayer was adjusted so that each approach cycle resulted in a depression force of ~1 nN before reproach (14). The reproach velocity was varied from 5 μm/s to 25 μm/s, and the dwell time between the cantilever and the bilayer was varied from 2 to 200 ms. We derived the rupture forces and corresponding loading rates from force-distance traces using IgorPro 4.09 software (Wavemetrics, Lake Oswego, OR; Fig. 1 *D*). For each considered receptor-ligand pair, rupture force measurements from >1000 successful binding events were first rank-ordered by the magnitude of the loading rate. Then, rupture forces from 50 rupture events of increasing magnitude were ensemble-averaged for rates up to 100 pN/s, and from 100 rupture events for rates > 100 pN/s (24,25). For each set of binned data, a mean adhesion force and loading rate were calculated and used to fit Bell model parameters. The Bell model parameters (the unstressed dissociation rate k°_{off} and the reactive compliance x_β) were tabulated by a least-squares fit to the linear region of a graph of rupture force against the logarithm of the loading rate (13–15).

Preparation of CD44-coated microspheres

Before protein binding was performed, 10-μm polystyrene microspheres (2.5×10^7 microspheres/ml; Bangs Labs, Fishers, IN) were washed three times with DPBS, followed by two washes with citrate-phosphate buffer (pH 3.0). After 1 h of incubation at room temperature (RT), the microspheres were washed once more with the citrate-phosphate buffer, three times with DPBS, and two times with binding buffer (0.2 M carbonate/bicarbonate buffer, pH 9.2). Immunoprecipitated CD44 from LS174T or HL60 whole-cell lysate was diluted to the desired concentrations with binding buffer and incubated with the microspheres overnight at 4°C with constant rotation. Microspheres were washed two times with DPBS and subsequently blocked with DPBS, 1% BSA for 1 h at RT. Subsequently, the microspheres were resuspended (2×10^6 microspheres/ml) in DPBS, 0.1% BSA for use in flow-based adhesion assays (16,20).

Flow-based adhesion assays

We prepared HA-coated surfaces by incubating 50 μg/ml HA with binding buffer on untreated 35-mm polystyrene suspension culture dishes overnight at 4°C. The plates were then washed with DPBS and blocked with 1% BSA for 1 h before they were used in flow-based adhesion assays. Suspensions of microspheres (2×10^6/ml) were perfused over HA-coated dishes using a parallel plate flow chamber (250 μm channel depth, 5.0 mm channel width). The microspheres were allowed to adhere and roll. Average rolling velocities were computed as the distance traveled by the centroid of the translating microsphere divided by the time interval at the given wall shear stress (19,20).

Statistics

The statistical significance of differences between means was determined by Student's *t*-test. Values of $p < 0.05$ were considered to be statistically significant.

RESULTS AND DISCUSSION

Comparison of the kinetic and micromechanical properties of CD44v-HA and CD44s-HA single bonds

HA is the major ligand for CD44. The HA-binding motif in the N-terminal domain of CD44, specifically amino acid residues 32–123, is common to both the standard and variant isoforms of CD44 (1). However, previous studies have shown that CD44v and CD44s bind HA with different efficiencies. Conflicting results indicate that CD44v binds HA with greater efficiency than CD44s (12), and vice versa (9–11). To eliminate the possibility that differential expression levels of CD44 dictated these conflicting data, we first performed a macroscopic cell-free, flow-based adhesion assay in which beads coated with an equivalent density of LS174T CD44v or HL60 CD44s molecules were perfused over immobilized HA substrates under flow. Both the CD44v- and CD44s-decorated microspheres adhered and exhibited similar rolling velocities on HA substrates at shear stress levels of 0.25 and 0.5 dyn/cm^2 (Fig. 2 *A*). The lack of dependence of the rolling velocity on shear stress has also been noted by other groups for shear stresses <1 dyn/cm^2 (26,27).

We next wished to compare the binding of HA to immunopurified LS174T CD44v relative to HL60 CD44s (Fig. 1 *C*) at the single-molecule level using short and long dwell times, thereby simulating the receptor-ligand encounter time at high (0.5 dyn/cm^2) and low (0.005 dyn/cm^2) shear regimes, respectively. CD44v or CD44s was reconstituted in DMPC lipid vesicles and then layered onto

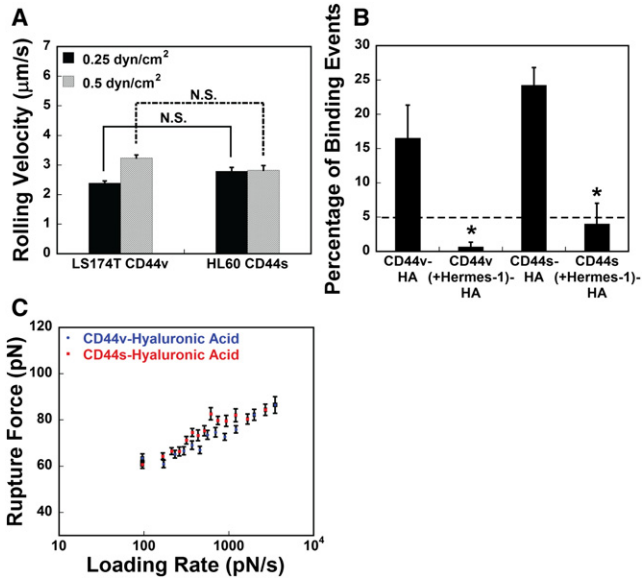

FIGURE 2 Kinetic and micromechanical properties of CD44-HA binding at the single-molecule level. (*A*) Average rolling velocities (μm/s) of microspheres (2×10^6/ml) decorated with either CD44v immunopurified from LS174T cells or CD44s immunopurified from HL60 cells on 50 μg/ml HA at prescribed wall shear stresses. Data represent the mean $\pm$ SE from $n = 3$ independent experiments. (*B*) Frequency of binding events between HA and CD44v or CD44s in the absence and presence of the function-blocking CD44 antibody Hermes-1. DMPC-CD44v or DMPC-CD44s lipid solutions were premixed with 20 μg/ml of the Hermes-1 mAb just before bilayers were formed on PEI-coated glass slides. Data represent the mean $\pm$ SE of $n = 3$ independent experiments; $^*p < 0.05$ with respect to control. (*C*) Rupture force (pN) as a function of loading rate (pN/s) for CD44v-HA and CD44s-HA interactions. Data were acquired for a range of retraction velocities from 5 to 25 μm/s, using a dwell time of 20 ms. Data represent the mean $\pm$ SE of $n = 4$–6 experiments, with each experiment having at least 1200 approach/reproach cycles.

a PEI-cushioned glass slide (15). The hydrophobic interactions between the lipid and the transmembrane domain of CD44 allowed it to be incorporated into the bilayer in the proper physiological orientation. In these experiments, we employed an MFP (Fig. 1 *B*). This device uses a small, flexible cantilever that deflects in response to forces generated between the HA-coated cantilever tip and CD44v or CD44s molecules incorporated into lipid bilayers when they are repeatedly brought into contact for 20 ms. As shown in representative force-distance traces, receptor-ligand unbinding at any given reproach velocity (5–25 μm/s) involved a single force step rather than multiple ones (Fig. 1 *D*). The prominent first peak in the force-distance traces of Fig. 1 *D* is due to nonspecific interactions occurring just after tip-substrate contact (commonly referred to as jump-off-contact) but before specific receptor-ligand unbinding (28). To further ensure that most binding events were mediated by a single receptor-ligand pair, we achieved a low probability (13) of binding (15–30%) by decorating the cantilever and lipid bilayers with dilute HA and CD44 concentrations, respectively. The function-blocking anti-CD44 mAb Hermes-1 abrogated the binding from ~20% down to baseline levels, suggesting that this is the primary binding site on CD44 for HA (Fig. 2 *B*).

The average rupture force of CD44v-HA and CD44s-HA bonds grew linearly with the natural log of the loading rate (Fig. 2 *C*). Moreover, the mean bond rupture forces at all loading rates were nearly identical for both receptor-ligand pairs. The Bell model parameters (i.e., the unstressed dissociation rate k°_{off} (s^{-1}) and reactive compliance x_β (nm)) were extracted from least-squares fits of the mean rupture force versus the logarithm of loading rate for HA binding to LS174T CD44v or HL60 CD44s (Fig. 2 *C*). The respective values for the off-rate and reactive compliance were also similar for the LS174T CD44v-HA (0.005 $\pm$ 0.003 s^{-1}, 0.59 $\pm$ 0.12 nm) and HL60 CD44s-HA (0.004 $\pm$ 0.002 s^{-1}, 0.55 $\pm$ 0.05 nm) pairs. From the experimentally calculated k°_{off} (s^{-1}) and x_β (nm), the Bell model based dissociation rate k_{off} was used to plot the bond lifetime ($1/k_{off}$) as a function of the applied force (see Fig. S1 in the Supporting Material). At 80 pN, the bond lifetime drops to 2 ms for the CD44v-HA pair, and to 5.4 ms for the CD44s-HA pair. Of note, the shear stress of 0.25 dyn/cm^2 corresponds to a hydrodynamic force of ~80 pN acting on a 10-μm PSGL-1-coated microsphere tethered on a selectin substrate (29,30). Taken together, the macroscopic flow-based adhesion assay and single-molecule force spectroscopy data reveal that CD44v and CD44s bind HA with similar affinity. Our data are supported by findings that the HA-binding site, which is common to CD44v and CD44s, is the primary binding site on CD44 because Hermes-1 nearly abrogates these binding interactions (Fig. 2 *B*). It is notable that the k°_{off} (s^{-1}) of CD44-HA binding is lower than that of CD44v-P-selectin (Table 1) (15). This helps explain the more stable and slower CD44-mediated rolling on HA compared with P-selectin substrates (31).

Roles of *O*- and *N*-glycosylation and sulfation in CD44-HA binding kinetics

Conflicting results regarding the effects of *O*-glycosylation of CD44 on its binding to HA have been obtained, depending on the cell types used and the method of stimulation

TABLE 1 Bell model parameters for CD44–counter-receptor interactions

Interaction	k°_{off} (s^{-1})	x_β (nm)
CD44v-P-selectin (15)	0.16 $\pm$ 0.03	0.36 $\pm$ 0.01
CD44v-fibrin (15)	0.43 $\pm$ 0.1	0.4 $\pm$ 0.05
CD44s-fibrin	0.44 $\pm$ 0.05	0.3 $\pm$ 0.01
CD44s-fibrinogen	0.62 $\pm$ 0.06	0.32 $\pm$ 0.02
CD44v-HA	0.005 $\pm$ 0.003	0.59 $\pm$ 0.12
CD44s-HA	0.004 $\pm$ 0.002	0.55 $\pm$ 0.05

Bell model parameters were tabulated by a least-squares fit to the linear region of the rupture force versus the logarithm of loading rate. Data are expressed as mean $\pm$ SD.

used in cells that do not constitutively bind HA (32). *O*-glycosylation has been shown to either positively or negatively regulate CD44-HA binding, or to not even affect it, in various cell lines (9,33–36). Force spectroscopy revealed that inhibition of *O*-glycosylation did not cause any significant alteration in the frequency of binding of CD44v or CD44s to HA at both of the contact durations tested, as well as at 20 ms (data not shown). These data are in line with findings showing that the HA binding motif on CD44 is the primary molecular constituent of CD44-HA interaction. Removal of *O*-linked glycans did not significantly alter the tensile strength of LS174T CD44v binding to HA (Fig. 3 *A*). However, this treatment caused a small but significant decrease in the tensile strength of CD44s binding to HA compared with the untreated control (Fig. 3 *B*). Our observations are in accord with others showing that *O*-linked glycans positively regulate the binding of CHO-CD44s-expressing cells (36). Taken together, our data suggest that although *O*-linked glycans are not indispensable, they play only an auxiliary role in CD44s-HA recognition.

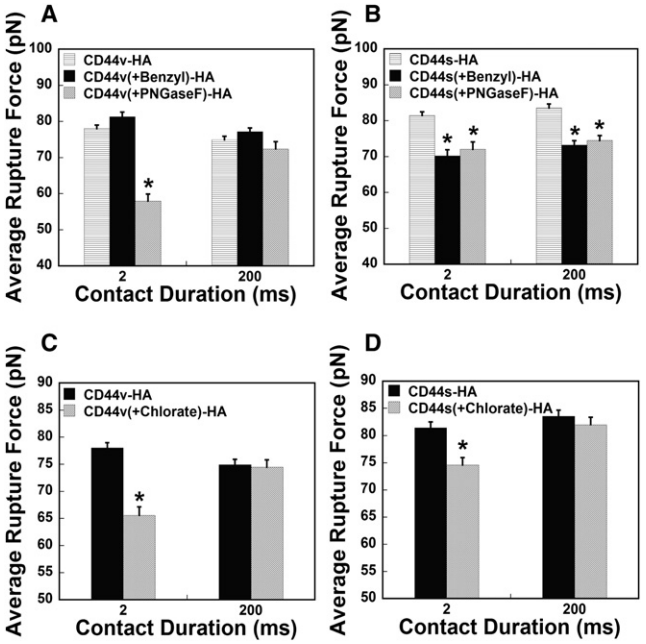

FIGURE 3 Role of glycosylation and sulfation of CD44 in CD44-HA binding. (*A* and *B*) Average rupture force of (*A*) CD44v-HA and (*B*) CD44s-HA as a function of contact duration. CD44v was immunoprecipitated from LS174T cells cultured in medium containing either 2 mM benzyl-GalNAc to inhibit *O*-linked glycosylation or DPBS. CD44s was immunoprecipitated from HL60 cells containing either 2 mM benzyl-GalNAc or DPBS. CD44v and CD44s were treated with PNGaseF according to the manufacturer's instructions to cleave *N*-linked glycans. (*C* and *D*) Average rupture force of (*C*) CD44v-HA and (*D*) CD44s-HA bonds as a function of contact duration. CD44v was immunoprecipitated from LS174T cells cultured in medium containing either sodium chlorate (60 mM) to block sulfation or DPBS. CD44s was immunoprecipitated from HL60 cells cultured in medium containing either sodium chlorate (20 mM) or DPBS. Data represent the mean ± SE of $n = 3$ independent experiments performed at a retraction velocity of 20 μm/s; $^*p < 0.05$ with respect to untreated control.

Previous investigators showed a positive correlation between *N*-linked glycans and CD44-HA binding in human lymphoma, melanoma cells, lung-epithelium-derived tumor cells expressing CD44s, and pancreatic cancer cells expressing CD44v (37–39). However, others reported either a negative correlation between *N*-glycosylation and CD44s-mediated HA binding on B-cells and monocytes (40,41) or no role for *N*-glycans in HA binding of CD44v-expressing colon carcinoma cells (33). In our work, enzymatic removal of *N*-linked oligosaccharides from the CD44 core protein did not affect the frequency of binding to HA, consistent with the notion that the HA-binding motif on CD44 is the primary molecular constituent of CD44-HA interaction. However, this intervention resulted in a significant reduction in the tensile strength of HL60 CD44s-HA binding at all contact times tested (Fig. 3 *B*). Interestingly, removal of *N*-linked glycans reduced the average rupture force of LS174T CD44v binding to HA only at the shorter (and not at the longer) contact duration (Fig. 3 *A*). Collectively, our results indicate that *N*-linked glycans contribute moderately to the tensile strength of CD44-HA binding during short (2 ms) dwell times that represent physiologically relevant flow conditions (0.5 dyn/cm^2). At longer dwell times (200 ms), there may be a compensatory mechanism to restore binding strength in the absence of *N*-linked glycans on CD44v.

We next investigated the potential role of sulfation in LS174T CD44v-HA and HL60 CD44s-HA binding. Blocking sulfation decreased the tensile strength of LS174T CD44v-HA and HL60 CD44s-HA binding compared with the untreated control at the shorter contact time, but not during long contact durations (Fig. 3, *C* and *D*). Similar results were previously obtained in studies of CD44s expressing peripheral blood monocytes, SR91 human leukemic cells, and L cell fibroblasts, indicating a positive correlation between sulfation and CD44-HA binding (42–44). Thus, our data suggest that sulfation contributes to the tensile strength of CD44-HA binding during short interaction times that represent physiologically relevant flow conditions. Given a sufficient encounter time between CD44 and HA, such as would occur under near-static conditions, there may be a compensatory mechanism to restore binding strength in the absence of CD44 sulfation. This may explain why the tensile strength was not significantly lower compared with that of the untreated control at the longer contact duration of 200 ms. These results further emphasize the predominant role played by the binding motif on the CD44 protein core (amino acid residues 32–123 in the N-terminal region) in mediating the strong binding with HA.

Kinetic and micromechanical properties of CD44s-fibrin versus CD44s-fibrinogen binding

We recently reported that CD44 is the major functional fibrin receptor on colon carcinoma cells (16,17). CD44s is

also capable of binding immobilized fibrin(ogen) (16). We thus wished to characterize the biophysics and molecular requirements of CD44s binding to fibrin(ogen). Force spectroscopy measurements reveal that the CD44s-fibrin bond displayed a significantly higher tensile strength than the CD44s-fibrinogen bond for loading rates $>$ 100 pN/s (Fig. 4 *A*). Moreover, the unstressed dissociation rate was significantly lower for CD44s-fibrin (0.44 ± 0.05 s^{-1}) than for the CD44s-fibrinogen bond (0.62 ± 0.06 s^{-1}), whereas modest differences were noted for the reactive compliance (Table 1). We validated the Bell model parameters by performing Monte Carlo simulations of bond rupture under constant loading rates (Fig. 4 *B*) (13,14). Of note, control experiments eliminated the possibility of CD44s-thrombin interactions in our force spectroscopy measurements (Fig. S2). Taken together, results indicate that the CD44s-fibrin bond is mechanically stronger than the CD44s-fibrinogen bond. These findings may explain the higher capability of CD44s-fibrin compared with CD44s-fibrinogen to mediate binding more efficiently at 0.5 dyn/cm^2 (16). Of note, the CD44s-fibrin(ogen) bonds are weaker than the CD44-HA pairs. Furthermore, CD44s-fibrin(ogen) bonds display a higher k°_{off} (s^{-1}) (Table 1) and a lower overall tensile strength in comparison with CD44v-P-selectin, which is in line with the ability of selectin-ligand interactions to mediate binding at higher hydrodynamic forces (15,19,20).

Blocking the HA-binding site on LS174T CD44v with Hermes-1 resulted in the abrogation of LS174T CD44v-fibrin binding compared with control (15). This finding suggests that the HA-binding motif on LS174T CD44v is critical for molecular recognition with fibrin, which is in agreement with macroscopic flow-based adhesion assays (16). Therefore, we sought to determine the effect of the presence of Hermes-1 mAb on CD44s-fibrin and CD44s-fibrinogen binding. Interestingly, no inhibitory effect was detected in the frequency of binding of CD44s to fibrin in the presence of Hermes-1 relative to the untreated control (Fig. 5 *A*), even though this antibody blockade caused a small reduction in the tensile strength of this receptor-ligand pair (Fig. 5 *B*). This finding suggests that the HA-binding site on CD44s makes a minor contribution to the recognition of fibrin, which is in stark contrast to its critical role in LS174T CD44v-fibrin binding (15,16). Surprisingly, this antibody treatment resulted in higher CD44s-fibrinogen rupture forces, especially at long dwell times (Fig. 5 *D*). These observations suggest that the HA-binding site modulates CD44s-fibrinogen binding, and that other molecular constituents on CD44s may be involved in the molecular recognition of fibrinogen. These constituents may remain cryptic during shorter contact durations. With an increase in the encounter time, they would be able to mediate more stable and stronger binding between CD44s and fibrinogen (Fig. 5 *D*). This finding may help explain the selective interaction between CD44s (but not CD44v) and immobilized fibrinogen (15,16). We speculate that the insertion of variant exons in the CD44 stem region might disrupt the three-dimensional structure of the fibrinogen-binding pocket on LS174T CD44 (16). Of note, increasing the dwell time from 2 to 200 ms did not affect the frequency of binding

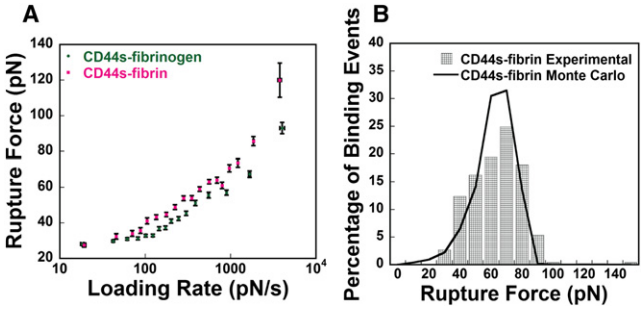

FIGURE 4 Kinetic and micromechanical properties of CD44s-fibrin and CD44s-fibrinogen interactions at the single-molecule level. (*A*) Rupture force (pN) as a function of loading rate (pN/s) for CD44s-fibrin and CD44s-fibrinogen interactions. Data were acquired for a range of retraction velocities from 5 to 25 μm/s and using a dwell time of 20 ms. Data represent mean $\pm$ SE of $n = 4$–6 experiments, where each experiment had at least 1200 approach/reproach cycles. (*B*) Distribution of adhesion forces obtained experimentally (*bars*) or computed using a Monte Carlo simulation (*line*) based on Bell model kinetic parameters for CD44s-fibrin interactions. The retraction velocity was maintained for 20 μm/s.

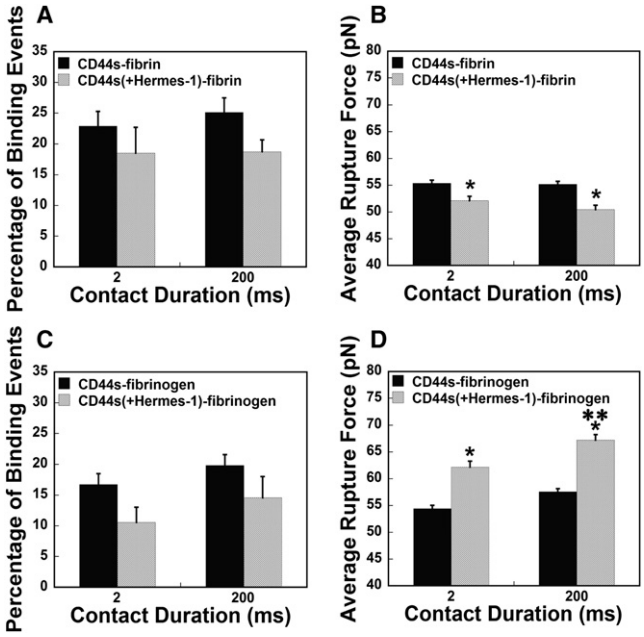

FIGURE 5 Effect of Hermes-1 on CD44s-fibrin(ogen) binding. (*A* and *B*) The frequency of binding events (*A*) and average rupture force (*B*) of CD44s binding to fibrin were evaluated in the absence and presence of the function-blocking CD44 antibody Hermes-1. (*C* and *D*) The frequency of binding events (*C*) and average rupture force (*D*) of CD44s binding to fibrinogen were evaluated in the absence and presence of Hermes-1. DMPC-CD44s lipid solutions were premixed with 20 μg/ml of the Hermes-1 mAb just before bilayers were formed on PEI-coated glass slides. Data represent the mean $\pm$ SE of $n = 3$ independent experiments; $^*p < 0.05$ with respect to untreated control, and $^{**}p < 0.05$ with respect to CD44s binding to fibrinogen in the presence of Hermes-1 at 2 ms.

events or the percentage of single or multiple CD44-ligand bonds as estimated by Poisson distribution statistics (Fig. S3, *A* and *B*) (15).

Roles of CS and DS in CD44-fibrin(ogen) binding

Treatment of immunopurified CD44s with chondroitinase ABC, which degrades all forms of CS and DS (2), essentially abolished the frequency of binding events between CD44s and fibrin(ogen) at both of the contact durations tested (Fig. 6, *A* and *B*). This finding reveals crucial roles of CS and/or DS in CD44s-fibrin(ogen) molecular recognition akin to their role in mediating LS174T CD44v-fibrin binding (15,16). Inhibition of *O*-glycosylation did not alter the frequency of CD44s-fibrin binding (Fig. S4 *B*), whereas treatment of immunopurified CD44s with PNGaseF nearly abrogated the binding to fibrin(ogen) to background levels, suggesting that the *N*-linked glycans displayed on CD44s are also responsible for its ability to bind to fibrin(ogen) (Fig. 6, *A* and *B*). In stark contrast, *O*-linked (but not *N*-linked) glycans play an important role in LS174T CD44v-fibrin binding (Fig. S4 *A*).

Although there was no significant alteration in the frequency of binding upon blocking sulfation on CD44s, this intervention decreased the tensile strength of CD44s-fibrinogen binding significantly at both dwell times (Fig. 6 *D*). This intervention reduced the rupture force of CD44s-fibrin binding at 2 ms (Fig. 6 *C*) but not at 200 ms. This observation at the longer dwell time highlights the difference in the binding of CD44s to fibrin versus fibrinogen. Moreover, the effect of blocking sulfation on CD44s-fibrin(ogen) binding is in distinct contrast to the marked increase in the tensile strength that is observed for CD44v-fibrin binding when sulfation is inhibited on LS174T CD44v (15,16). Thus, it is possible that the negatively charged sulfate groups on CD44s, particularly on the stretches of CS and/or DS GAGs, facilitate the binding to positively charged regions of the fibrin(ogen) molecule during short interaction times. On the other hand, when the negatively charged sulfate groups are removed from CD44v, the stretches of unsulfated CS and/or DS GAGs may bind to negatively charged regions of the fibrin molecule to facilitate strong binding even at short contact durations (15). Our studies further emphasize the role played by GAGs in primarily mediating the binding to fibrin(ogen), which suggests that the HA-binding motif on the CD44s molecule plays a modest role in fibrin(ogen) recognition. This phenomenon is in contrast to CD44-HA binding, wherein the HA-binding motif plays the greater role in mediating molecular recognition when compared with the glycans.

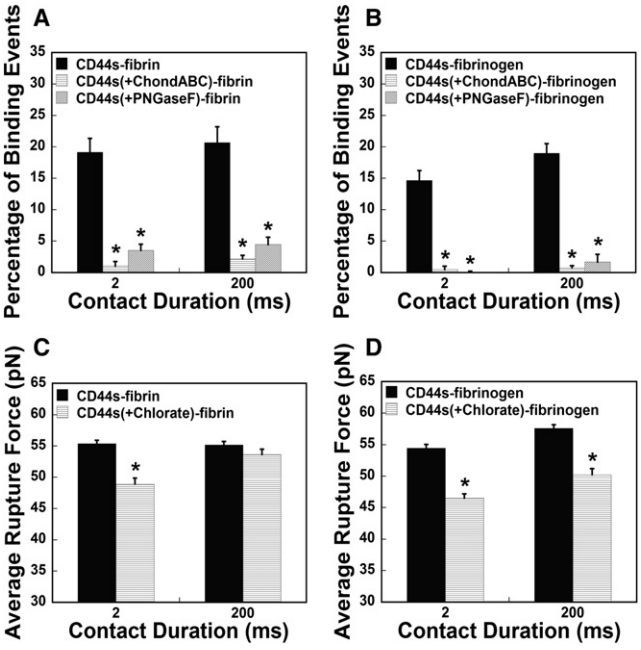

FIGURE 6 Role of glycosylation and sulfation of CD44 in CD44-fibrin(ogen) binding. (*A* and *B*) Frequency of binding between CD44s treated with chondroitinase ABC (1 U/ml) or PNGaseF according to the manufacturer's instructions, and (*A*) fibrin or (*B*) fibrinogen as a function of contact duration compared with untreated control. (*C* and *D*) Average rupture force of (*C*) CD44s-fibrin and (*D*) CD44s-fibrinogen bonds as a function of contact duration. CD44s was immunoprecipitated from HL60 cells cultured in medium containing sodium chlorate (20 mM) to block sulfation or DPBS. Data represent the mean ± SE of $n = 3$ independent experiments performed at a retraction velocity of 20 μm/s; $^*p < 0.05$ with respect to untreated control.

The CD44s-binding site on fibrin is localized in the (β15–66) regions forming fibrin βN-domains (16). Although CD44s-coated microspheres interact efficiently with the $(B\beta 1–66)_2$ fragment, which mimics fibrinogen, at a low shear stress level of 0.25 dyn/cm^2, no binding was detected between soluble fibrinogen and immobilized CD44s in previous surface plasmon resonance assays (16). Fibrinogen immobilization could result in the exposure of a cryptic binding site that is capable of mediating binding to CD44s but not CD44v (16). In addition, removal of the fibrinopeptide B by thrombin during conversion of fibrinogen to fibrin could make the binding site more accessible to CD44s. This could also help explain the differences in kinetic and micromechanical properties observed between CD44s-fibrin and CD44s-fibrinogen binding.

CONCLUDING REMARKS

In summary, we have characterized the kinetic and micromechanical properties of CD44–counter-receptor interactions at the single-molecule level using a combination of force spectroscopy, which has the benefit of being highly quantitative, and biochemical tools such as enzymatic treatments and metabolic inhibitors to eliminate the potential contribution of subtle differences of expression levels. Our study may help reconcile the differences documented in the literature regarding CD44 binding to HA. Also, our findings provide insight into the nanomechanical functions of CD44 with HA and fibrin(ogen), which play key roles in

important (patho)physiological processes such as inflammation and cancer metastasis.

SUPPORTING MATERIAL

Four figures are available at http://www.biophysj.org/biophysj/supplemental/S0006-3495(12)00728-X.

This work was supported by the National Institutes of Health (NCI R01 CA101135 and U54 CA143868), a Kleberg award, and a predoctoral fellowship from the American Heart Association (to P.R.).

REFERENCES

1. Ponta, H., L. Sherman, and P. A. Herrlich. 2003. CD44: from adhesion molecules to signalling regulators. *Nat. Rev. Mol. Cell Biol.* 4:33–45.
2. Clark, R. A., F. Lin, …, J. R. Couchman. 2004. Fibroblast invasive migration into fibronectin/fibrin gels requires a previously uncharacterized dermatan sulfate-CD44 proteoglycan. *J. Invest. Dermatol.* 122:266–277.
3. Greenfield, B., W. C. Wang, …, K. L. Bennett. 1999. Characterization of the heparan sulfate and chondroitin sulfate assembly sites in CD44. *J. Biol. Chem.* 274:2511–2517.
4. Takahashi, K., I. Stamenkovic, …, K. K. Tanabe. 1996. Keratan sulfate modification of CD44 modulates adhesion to hyaluronate. *J. Biol. Chem.* 271:9490–9496.
5. Mohamadzadeh, M., H. DeGrendele, …, M. Siegelman. 1998. Proinflammatory stimuli regulate endothelial hyaluronan expression and CD44/HA-dependent primary adhesion. *J. Clin. Invest.* 101:97–108.
6. Nandi, A., P. Estess, and M. H. Siegelman. 2000. Hyaluronan anchoring and regulation on the surface of vascular endothelial cells is mediated through the functionally active form of CD44. *J. Biol. Chem.* 275:14939–14948.
7. Lesley, J., R. Hyman, …, G. A. Turner. 1997. CD44 in inflammation and metastasis. *Glycoconj. J.* 14:611–622.
8. Johnson, P., A. Maiti, …, R. Li. 2000. A role for the cell adhesion molecule CD44 and sulfation in leukocyte-endothelial cell adhesion during an inflammatory response? *Biochem. Pharmacol.* 59:455–465.
9. Bennett, K. L., B. Modrell, …, A. Aruffo. 1995. Regulation of CD44 binding to hyaluronan by glycosylation of variably spliced exons. *J. Cell Biol.* 131:1623–1633.
10. Jackson, D. G., J. I. Bell, …, N. Whittle. 1995. Proteoglycan forms of the lymphocyte homing receptor CD44 are alternatively spliced variants containing the v3 exon. *J. Cell Biol.* 128:673–685.
11. Stamenkovic, I., A. Aruffo, …, B. Seed. 1991. The hematopoietic and epithelial forms of CD44 are distinct polypeptides with different adhesion potentials for hyaluronate-bearing cells. *EMBO J.* 10:343–348.
12. Sleeman, J. P., S. Arming, …, P. Herrlich. 1996. Hyaluronate-independent metastatic behavior of CD44 variant-expressing pancreatic carcinoma cells. *Cancer Res.* 56:3134–3141.
13. Hanley, W., O. McCarty, …, K. Konstantopoulos. 2003. Single molecule characterization of P-selectin/ligand binding. *J. Biol. Chem.* 278:10556–10561.
14. Hanley, W. D., D. Wirtz, and K. Konstantopoulos. 2004. Distinct kinetic and mechanical properties govern selectin-leukocyte interactions. *J. Cell Sci.* 117:2503–2511.
15. Raman, P. S., C. S. Alves, …, K. Konstantopoulos. 2011. Single-molecule binding of CD44 to fibrin versus P-selectin predicts their distinct shear-dependent interactions in cancer. *J. Cell Sci.* 124:1903–1910.
16. Alves, C. S., S. Yakovlev, …, K. Konstantopoulos. 2009. Biomolecular characterization of CD44-fibrin(ogen) binding: distinct molecular requirements mediate binding of standard and variant isoforms of CD44 to immobilized fibrin(ogen). *J. Biol. Chem.* 284:1177–1189.
17. Alves, C. S., M. M. Burdick, …, K. Konstantopoulos. 2008. The dual role of CD44 as a functional P-selectin ligand and fibrin receptor in colon carcinoma cell adhesion. *Am. J. Physiol. Cell Physiol.* 294:C907–C916.
18. Konstantopoulos, K., and S. N. Thomas. 2009. Cancer cells in transit: the vascular interactions of tumor cells. *Annu. Rev. Biomed. Eng.* 11:177–202.
19. Hanley, W. D., S. L. Napier, …, K. Konstantopoulos. 2006. Variant isoforms of CD44 are P- and L-selectin ligands on colon carcinoma cells. *FASEB J.* 20:337–339.
20. Napier, S. L., Z. R. Healy, …, K. Konstantopoulos. 2007. Selectin ligand expression regulates the initial vascular interactions of colon carcinoma cells: the roles of CD44v and alternative sialofucosylated selectin ligands. *J. Biol. Chem.* 282:3433–3441.
21. Erb, E. M., and J. Engel. 2000. Reconstitution of functional integrin into phospholipid vesicles and planar lipid bilayers. *Methods Mol. Biol.* 139:71–82.
22. Cheung, L. S., M. Kanwar, …, K. Konstantopoulos. 2012. A hot-spot motif characterizes the interface between a designed ankyrin-repeat protein and its target ligand. *Biophys. J.* 102:407–416.
23. Lamontagne, C. A., and M. Grandbois. 2008. PKC-induced stiffening of hyaluronan/CD44 linkage; local force measurements on glioma cells. *Exp. Cell Res.* 314:227–236.
24. Bajpai, S., J. Correia, …, D. Wirtz. 2008. α-Catenin mediates initial E-cadherin-dependent cell-cell recognition and subsequent bond strengthening. *Proc. Natl. Acad. Sci. USA.* 105:18331–18336.
25. Bajpai, S., Y. Feng, …, D. Wirtz. 2009. Loss of α-catenin decreases the strength of single E-cadherin bonds between human cancer cells. *J. Biol. Chem.* 284:18252–18259.
26. Gal, I., J. Lesley, …, K. Mikecz. 2003. Role of the extracellular and cytoplasmic domains of CD44 in the rolling interaction of lymphoid cells with hyaluronan under physiologic flow. *J. Biol. Chem.* 278:11150–11158.
27. Ogino, S., N. Nishida, …, I. Shimada. 2010. Two-state conformations in the hyaluronan-binding domain regulate CD44 adhesiveness under flow condition. *Structure.* 18:649–656.
28. Cappella, B., and G. Dietler. 1999. Force-distance curves by atomic force microscopy. *Surf. Sci. Rep.* 34:1–104.
29. Cheung, L. S., and K. Konstantopoulos. 2011. An analytical model for determining two-dimensional receptor-ligand kinetics. *Biophys. J.* 100:2338–2346.
30. Yago, T., J. Wu, …, R. P. McEver. 2004. Catch bonds govern adhesion through L-selectin at threshold shear. *J. Cell Biol.* 166:913–923.
31. McCarty, O. J., S. A. Mousa, …, K. Konstantopoulos. 2000. Immobilized platelets support human colon carcinoma cell tethering, rolling, and firm adhesion under dynamic flow conditions. *Blood.* 96:1789–1797.
32. Jacobs, P. P., and R. Sackstein. 2011. CD44 and HCELL: preventing hematogenous metastasis at step 1. *FEBS Lett.* 585:3148–3158.
33. Dasgupta, A., K. Takahashi, …, K. K. Tanabe. 1996. O-linked glycosylation modifies CD44 adhesion to hyaluronate in colon carcinoma cells. *Biochem. Biophys. Res. Commun.* 227:110–117.
34. Lokeshwar, V. B., and L. Y. Bourguignon. 1991. Post-translational protein modification and expression of ankyrin-binding site(s) in GP85 (Pgp-1/CD44) and its biosynthetic precursors during T-lymphoma membrane biosynthesis. *J. Biol. Chem.* 266:17983–17989.
35. Nakano, T., T. Matsui, and T. Ota. 1996. Benzyl-α-GalNAc inhibits sialylation of O-glycosidic sugar chains on CD44 and enhances experimental metastatic capacity in B16BL6 melanoma cells. *Anticancer Res.* 16(6B):3577–3584.
36. Skelton, T. P., C. Zeng, …, I. Stamenkovic. 1998. Glycosylation provides both stimulatory and inhibitory effects on cell surface and soluble CD44 binding to hyaluronan. *J. Cell Biol.* 140:431–446.

37. Bartolazzi, A., A. Nocks, …, I. Stamenkovic. 1996. Glycosylation of CD44 is implicated in CD44-mediated cell adhesion to hyaluronan. *J. Cell Biol.* 132:1199–1208.

38. Cichy, J., and E. Pure. 2000. Oncostatin M and transforming growth factor-β1 induce post-translational modification and hyaluronan binding to CD44 in lung-derived epithelial tumor cells. *J. Biol. Chem.* 275:18061–18069.

39. Sleeman, J., W. Rudy, …, H. Ponta. 1996. Regulated clustering of variant CD44 proteins increases their hyaluronate binding capacity. *J. Cell Biol.* 135:1139–1150.

40. Hathcock, K. S., H. Hirano, …, R. J. Hodes. 1993. CD44 expression on activated B cells. Differential capacity for CD44-dependent binding to hyaluronic acid. *J. Immunol.* 151:6712–6722.

41. Levesque, M. C., and B. F. Haynes. 1999. TNFα and IL-4 regulation of hyaluronan binding to monocyte CD44 involves posttranslational modification of CD44. *Cell. Immunol.* 193:209–218.

42. Brown, K. L., A. Maiti, and P. Johnson. 2001. Role of sulfation in CD44-mediated hyaluronan binding induced by inflammatory mediators in human CD14(+) peripheral blood monocytes. *J. Immunol.* 167:5367–5374.

43. Esford, L. E., A. Maiti, …, P. Johnson. 1998. Analysis of CD44 interactions with hyaluronan in murine L cell fibroblasts deficient in glycosaminoglycan synthesis: a role for chondroitin sulfate. *J. Cell Sci.* 111:1021–1029.

44. Maiti, A., G. Maki, and P. Johnson. 1998. TNF-α induction of CD44-mediated leukocyte adhesion by sulfation. *Science.* 282:941–943.

Distinct Kinetic and Molecular Requirements Govern CD44 Binding to Hyaluronan versus Fibrin(ogen)

Phrabha S. Raman, Christina S. Alves, Denis Wirtz, Konstantinos Konstantopoulos

Supplementary Information

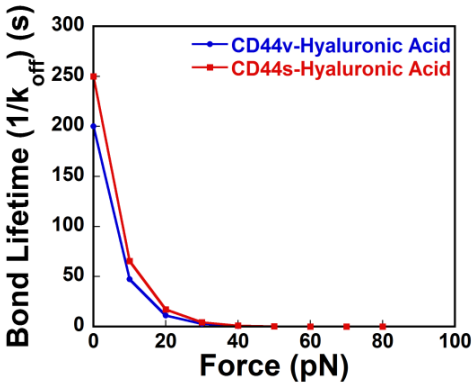

Fig. S1: Force dependence of the CD44-HA bond lifetime. From the experimentally calculated $k°_{off}$ (s^{-1}) and x_β (nm), the Bell model based dissociation rate k_{off} was used to plot the bond lifetime ($1/k_{off}$) as a function of the applied force.

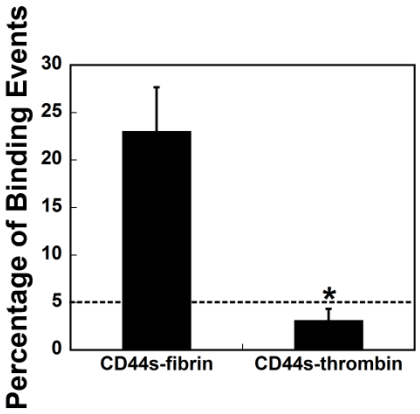

Fig. S2: Specificity of CD44s-fibrin binding. Frequency of binding events between CD44s and thrombin treated fibrinogen (fibrin) or thrombin alone. Data represent the mean ± SE of n=3 independent experiments performed at a retraction velocity of 20 μm/s. *P<0.05 with respect to CD44s-fibrin.

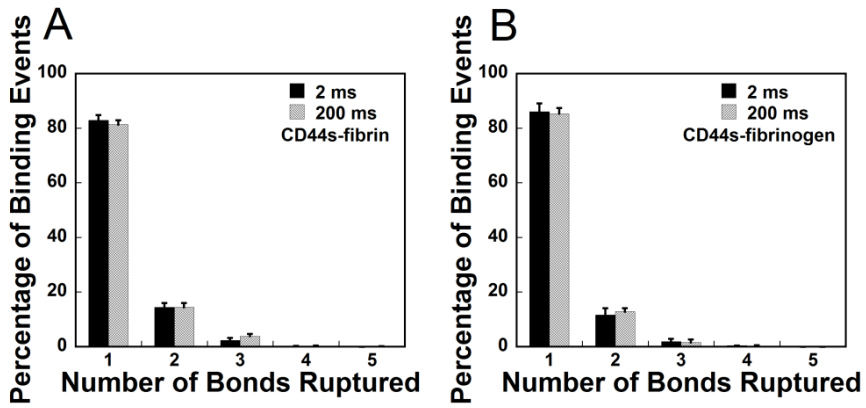

Fig. S3: Single molecule CD44s-fibrin and CD44s-fibrinogen binding. Percentage of single or multiple *(A)* CD44s-fibrin and *(B)* CD44s-fibrinogen bonds as a function of contact duration. The distribution obeys Poisson statistics. Data represent mean ± SE of n=3 independent experiments.

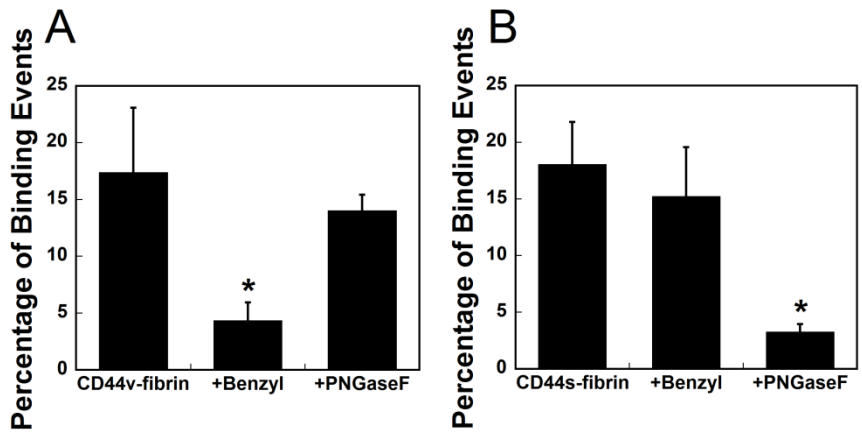

Fig. S4: Effect of glycosylation on CD44-fibrin binding. Percentage of binding events of *(A)* CD44v-fibrin and *(B)* CD44s-fibrin. CD44v was immunoprecipitated from LS174T cells cultured in medium containing either 2 mM benzyl-GalNAc to inhibit *O*-linked glycosylation or DPBS. CD44s was immunoprecipitated from HL60 cells containing either 2 mM benzyl-GalNAc or DPBS. Immunoprecipitated CD44v and CD44s were treated with PNGaseF according to the manufacturer's instructions to cleave *N*-linked glycans. Data represent mean ± SE of n=3 independent experiments. *P<0.05 with respect to untreated control.